The role of the annealing temperatures on the structure and optical properties of Rose Bengal thin films

H. M. Zeyada, M. I. Youssif, N. A. El-Ghamaz, M. E. O. Aboderbala

Abstract— Uniform thin films of Rose Bengal, RB, have been successfully prepared by the spin coating technique. Results of thermal analysis for RB films showed its stability up to 514 K. Fourier transform infrared (FTIR) measurements proved no changes occurred in the chemical bonds of RB films upon annealing. X-ray diffraction showed that the powder, the pristine and the annealed (363 K) thin films of RB have amorphous structure. The amorphous pristine films become polycrystalline structure after being annealed at 423 K. Optical properties of pristine and annealed RB films have been investigated using transmittance and reflectance methods. The refractive index (n) and the extinction coefficient (k) of RB films were directly calculated from the absolute values of the transmission and the reflection spectra. Single oscillator parameters and Drude model of free carrier absorption have been applied for the analysis of refractive index dispersion. The optical absorption edge data were analyzed within the frame work of the band-to-band electron transitions theory. Annealing temperatures created variations in the absorption coefficient, the energy gap and the refractive index of RB films. The optical functions and their dependence on the annealing temperatures were directly calculated from the spectral distribution of dielectric constant.

Index Terms— Absorption Characteristics, Annealing Temperatures, Dispersion, Optical Functions, Optical Properties, Rose Bengal, Thin Films.

1 INTRODUCTION

Rose Bengal, 2,4,5,7- tetraiodo- 3',4',5',6'- tetrachlofluorescein (C. I. name is Acid Red 94) is a tetraiodo-substituted dye of the xanthenes class of dyes. RB has a molecular formula $C_{20}H_2Cl_4I_4Na_2O_5$ and its molecular structure is shown in Fig.1. RB demonstrates at least six distinct electronic properties [1] which are otherwise hidden in the molecule. RB is a double planar molecule and relative rotation of the planes generates unique electronics. Therefore, RB is a suitable candidate for molecular electronics. It has potential applications in bulk heterojunction solar cells [2]; and dye-sensitized solar cells [3, 4]. Moreover, it is used as photo sensitizer for the enhancement of conversion efficiency and storage capacity of photo galvanic cell [5]. It sensitized TiO_2 film electrode [6]; Rose Bengal water solutions quenched by potassium iodide can be used to measure instrument response functions of single photon detectors in the orange-red wavelength region [7]. Furthermore, RB is used as photo sensitizer in dye sensitized photo chemical cells [8, 9] and it also has chemical, medical and biological applications [10-12]. However, the details about RB optical constants and their spectral response in bulk form and thin film conditions have not been reported.

The arrangement of molecules during the film growth strongly depends on the growth conditions, kind of substrates, as well as the thermal processes applied immediately after the thin film deposition. The knowledge of the linear and nonlinear optical properties is extremely important for applications of RB in modern optical technologies. Nonlinear optical materials with large susceptibility (second and third order) are essential for light emitting, modulating, and information technology devices because they determine the efficiency of these devices.

In this work, we report for the first time, the influence of annealing temperatures on the structure, optical and dielectrical properties and optical functions of RB films prepared by the spin coating technique.

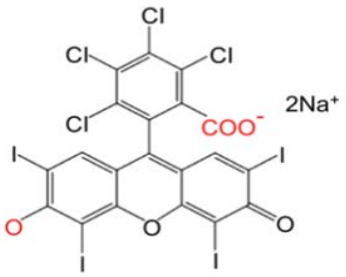

Fig. 1. The molecular structure of Rose Bengal.

2 EXPERIMENTAL PROCEDURE

RB was obtained from Aldrich and is used as it supplied. The as-received RB dye in a powder form with different weights of 40, 50, 75, 100 and 175 mg were individually dis-

- *H. M. Zeyada is currently a Professor of Physics in Department of Physics, Faculty of Science at New Damietta, University of Damietta, New Damietta 34517, Egypt. E-mail: hzeyada@gmail.com*
- *M. I. Youssif is currently an Assoc. Professor of Physics in Department of Physics, Faculty of Science at New Damietta, University of Damietta, New Damietta 34517, Egypt. E-mail: youssifm@yahoo.com*
- *N. A. El-Ghamaz is currently an Assoc. Professor of Physics in Department of Physics, Faculty of Science at New Damietta, University of Damietta, New Damietta 34517, Egypt. E-mail: elghamaz@yahoo.com*
- *M. E. O. Aboderbala is currently pursuing master's degree program in Physics in Faculty of Science at New Damietta, University of Damietta, New Damietta 34517, Egypt. She is working at Department of Physics, Faculty of Science, AlJabl Al Gharbi University, Libya. E-mail: aboderbala81@gmail.com*

solved in 5 mL of absolute ethanol and filtered. Homogenous thin films of RB are prepared by a conventional spin coating technique onto pre-cleaned optical flat quartz substrates at room temperature for optical measurements and onto pre-cleaned KBr substrates for FTIR measurements. The Thermal analyses measurements (thermo gravimetric, TGA, differential thermo gravimetric, DTGA, and differential scanning calorimetric, DSC) of RB films is performed using "NETZSCH STA 409 C/CD, Japan" under flowing He with flow rate (1 ml/min) on platinum crucible with a heating rate of 8 °C/min from ambient temperature to 600 °C, and the reference mass is 18 mg of Al_2O_3. Cleaned ordinary glass slides were used as substrates for depositing films for X-ray diffraction, XRD, analysis. The substrates are fixed to the stage of the spin coater and the rotating speed is controlled to be about 2800 rpm. The film thickness is determined optically by Lloyd's method [13]. The thickness of the produced thin films is found to be 250 nm. The films were annealed in a tubular dark furnace at 363 and 423 K with soaking time of 30 min. Fourier transform infrared, FTIR, spectra are recorded using Perkin-Elmer 1340 Spectrophotometer. The structural analysis of the powder and thin films is performed at room temperature using X-ray diffraction system (Philips X' pert) with filtered CuKα-radiation (λ = 1.5405 Å). The diffraction system was used to investigate the formed phase in the angle range 4–60°. The applied voltage and tube current were 40 kV and 30 mA, respectively. The measurements of the transmittance, $T(\lambda)$, and reflectance, $R(\lambda)$, of thin films are carried out at room temperature at nearly normal incidence of light in the wavelength range 200-2500 nm in steps of 2 nm using a double-beam spectrophotometer (JASCO model V-570-UV/vis./NIR). The absolute values of $T(\lambda)$ and $R(\lambda)$ are used to calculate the optical constants according to the relations [14]:

$$T(\lambda) = \left(\frac{I_{ft}}{I_q}\right)(1 - R_q) \quad (1)$$

$$R(\lambda) = \left(\frac{I_{fr}}{I_{Al}}\right)R_{Al}\left[1 + (1 - R_q)^2\right] - T^2 R_q \quad (2)$$

The parameter I_{ft} and I_q are the intensities of the light passing through film quartz system and the reference quartz substrate, respectively. The intensities of the light reflected from the sample and from the reference mirror are I_{fr} and I_{Al}, respectively. The reflectance of Al mirror is R_{Al}, and R_q is the reflectance of the quartz substrate.

The refractive index, n, absorption index, k, and absorption coefficient, a can be calculated using the absolute values $R(\lambda)$ and $T(\lambda)$ according to the following relations [15]:

$$\alpha = \left(\frac{1}{d}\right)\ln\left[\frac{(1-R)^2}{2T} + \sqrt{\frac{(1-R)^4}{4T^2} + R^2}\right] \quad (3)$$

$$k = \frac{\alpha\lambda}{4\pi} \quad (4)$$

where d is the thickness of the film and λ is the wavelength of the incident light on the sample. The refractive index, n, can be calculated by using the relation [16]:

$$n = \frac{(1+R)}{(1-R)} + \sqrt{\left(\left(\frac{4R}{(1-R)^2}\right) - k^2\right)} \quad (5)$$

Since the thickness of the film (d) is previously determined, then the computation can be carried out and the values of n, k and a can be obtained. The experimental errors are taken into account as follows: ±1% for T and R calculations, ±3% for refractive index, ±2.5% for absorption index and ±2.5% for film thickness measurements [17].

3 RESULTS

3.1 Structural Analysis

A comparative study of the FTIR spectra for the as received RB powder, RB in the pristine thin film form and annealed (423 K with soaking time of 30 min.) thin film condition is shown in Fig. 2. The absorption peaks are assigned and listed in Table 1.

The thermographs of RB are shown in Fig. 3. From DTGA and DSC curves, we can see that there are two mass loss steps at the temperature ranges from 300-357 K and from 608-673 K. The first loss of mass can be attributed to the loss of moisture from the sample. The second loss of mass can be attributed to the decomposition of RB [18, 19]. The DTGA curve in Fig. 3 shows that RB has a constant rate of mass loss in the temperature range 357-498 K. The DSC curve shows an endothermic peak at 357 K, an exothermic peak at 598K and a plateau at 642-680 K. The glass temperature T_g (357 K) as defined by the endothermic change in the DSC trace indicates a large change of viscosity, marking a transformation from an amorphous solid phase to the super cooled liquid state. The exothermic peak temperature T_c (598 K) is used to identify the melting temperature. The plateau at 642-680 K, defines the decomposition temperature. Annealing temperatures of RB films was performed at 363 K which is a little pit near from the glass transition temperature T_g (357 K), and at 423 K that place in between the glass transition temperature and the melting temperature.

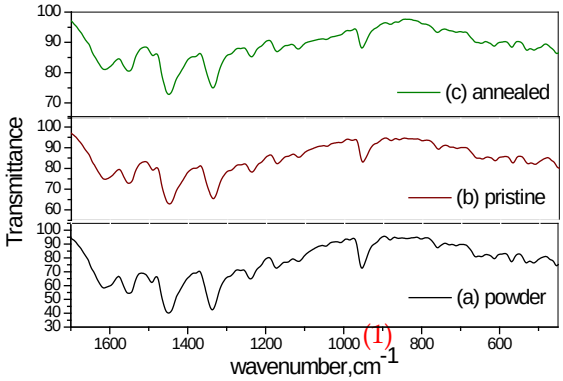

Fig. 2. FTIR spectra of RB, (a) powder form, (b) pristine film and (c) annealed film at 423 K with 0.5 h soaking time.

The average crystallite size, D, can be calculated by using the well-known Scherer's equation [20]:

TABLE 1
ASSIGNMENT OF TRANSMISSION PEAKS FOR RB IN POWDER, PRISTINE AND ANNEALED FILM AT 423 K WITH 0.5 H SOAKING TIME.

Powder $\bar{\nu}$ (cm^{-1})	Pristine film $\bar{\nu}$ (cm^{-1})	Annealed film at 423K $\bar{\nu}$ (cm^{-1})	Assignment
456.29	451.422	456.90	**C — I**
516.33	511.46	516.33	**C —Cl**
567.44	567.44	567.44	**C — Cl**
614.51	614.51	614.51	**C — Cl**
657.51	657.51	653.456	**C — Cl**
760.55	760.55	760.55	**C — Cl**
952.855	952.85	949.79	**C— C stretching vibration**
1120.81	1115.94	1120.18	**C — H in plane bending vibration**
1171.2	1171.92	1171.92	**C — H in plane bending vibration**
1244	1240.08	1236.02	**C — H in plane bending vibration**
1335.015	1339.07	1335.01	**C=C stretching vibration**
1455.1	1450.23	1455.23	**C=C stretching vibration**
1493.23	1489.17	1493.23	**C=C stretching vibration**
1549.22	1553.27	1553.27	**C=C stretching vibration**
1613.37	1617.31	1617.37	**C=O stretching vibration**

$$D = \frac{0.95\,\lambda}{\gamma \cos\theta} \qquad (6)$$

where γ is the width, measured in radians, of the half-maximum peak intensity, λ is the x-ray wavelength and θ is the Bragg's diffraction angle.

The x-ray diffraction, XRD, patterns of RB in the powder from, pristine and annealed thin films (annealing temperatures are 363 and 423 K with a soaking time of 30 min.) are shown in Fig. 4. As can be observed from Fig. 4 (a, b and c), there is a halo around $2\theta \approx 25^{o}$ indicating that both of the powder, the pristine and annealed (363 K for 30 min.) thin films of RB have amorphous structure. Fig. 4d shows that the amorphous structure of the annealed (363 K for 30 min.) thin film crystallizes into a single crystalline phase upon annealing at 453 K for 30 min. The determined crystallite size is 232 nm.

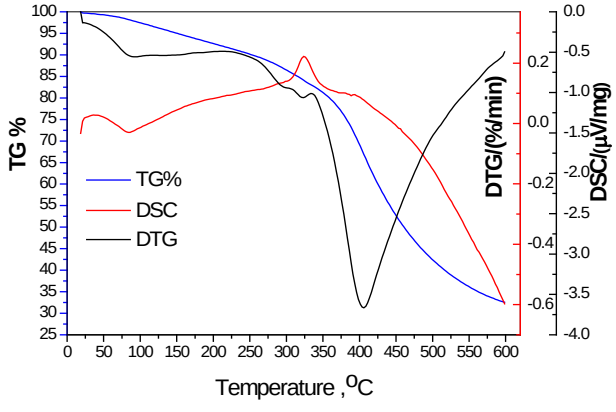

Fig. 3. Differential scanning calorimeter (DSC), thermal gravimetric (TG) and its derivative (DTG) curves of RB.

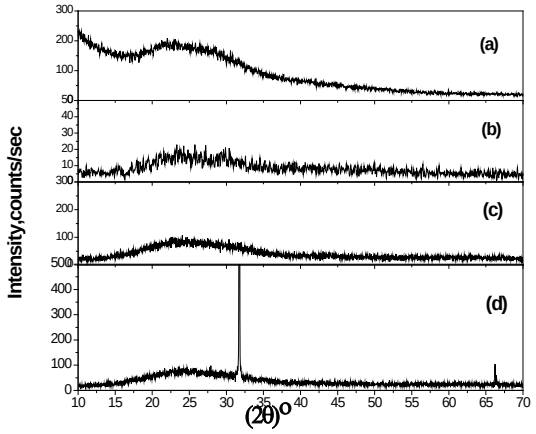

Fig. 4. XRD patterns of RB; (a) powder form, (b) pristine film, (c) annealed film at 363 K and (d) annealed film at 423 K with 0.5 h soaking time.

3.2 Optical Properties

For Fig. 5 illustrates the effects of annealing temperatures, 300-453 K with soaking time of 30 min., on the spectral behavior of $T(\lambda)$ and $R(\lambda)$ for the RB thin film of thickness 250 nm. Generally, the annealing process reduces the values of T and R all over the spectra. No new peaks are observed in the spectra of T and R in absorption region. Therefore, the annealing temperatures have not change the transmittance and reflectance properties of the films. We can also notice a transmission band in the wavelength range 315-495 nm and a sharp absorption edge at 579 nm, the integrated intensity of the transmission band depends on the annealing temperature.

Fig. 6 demonstrates the spectral distribution of refractive index, n, and extinction coefficient, k, for annealed RB thin films. The spectral behavior of n shows normal dispersion at $\lambda > 600$ nm and anomalous dispersion at $\lambda < 600$ nm. The dispersion curve shows two dispersion peaks and two shoulders in the ultraviolet and visible region of spectra.

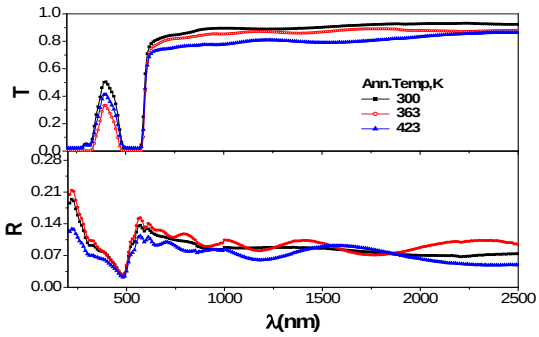

Fig. 5. The spectral distribution of transmittance, $T(\lambda)$ and reflectance, $R(\lambda)$ for annealed RB thin films.

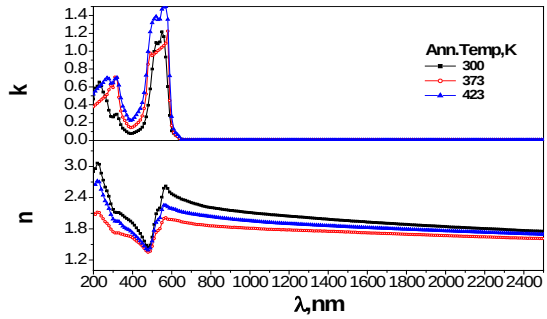

Fig. 6. The spectral distribution of refractive index, *n*, and extinction coefficient, *k*, for annealed RB thin films.

Generally, we have found that the annealing temperatures reduce the value of *n* all over the spectrum. The extinction coefficient curves show four peaks, two of them are in the ultraviolet region of spectra and the other two are in the visible region. The absorption peaks are assigned to 230, 320, 521 and 547 nm. Annealing at 363 K merges the two peaks at 230 and 320 nm into one peak at 315 nm, a shoulder appeared in the wavelength range 509-569 nm, and it also decreases the value of extinction coefficient all over the spectrum. Annealing at 463 K increases the value of *k* all over the spectrum and shifts peaks positions towards the high wavelength values.

3.2.1 Absorption Characteristics of Annealed RB Films

The spectral dependence of the absorption coefficient, *a*, for the annealed RB thin films in comparison with that of pristine RB thin film is presented in Fig. 7.

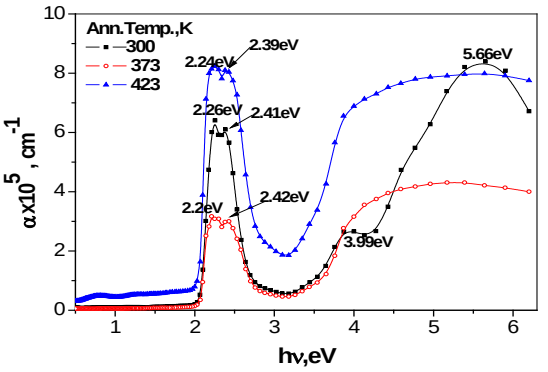

Fig. 7. Effect of annealing temperatures on the spectral distribution of absorption coefficient, α, of RB thin films.

The distribution of absorption coefficient, *a*, shows a different response to the annealing temperatures; annealing at 363 K for 30 min reduces the value of *a* all over the spectrum although annealing at 423 K for 30 min increases the value of *a*, all over the spectrum.

The dependence of the absorption coefficient of a material on the incident photon energy has been formulated by Tauc's relation [21] as:

$$\alpha h\nu = B\left(h\nu - E_g\right)^x \qquad (7)$$

the parameter *B* is a constant related to the electronic transition probability and *x* is the power which characterizes the type of transition process, *x* = 1/2 and 3/2 for direct allowed and forbidden transitions, respectively, and *x* = 2 and 3 for indirect allowed and forbidden transitions, respectively. The best fit for the data is found to be with the value of *x* = 2, indicating that the dominant transition is indirect allowed one. Fig. 8, illustrates the spectral distribution of $(ahv)^{1/2}$ as a function of incident photon energy. The value of the energy gap is obtained by extrapolating straight portion of the curve to intercept the abscissa axis.

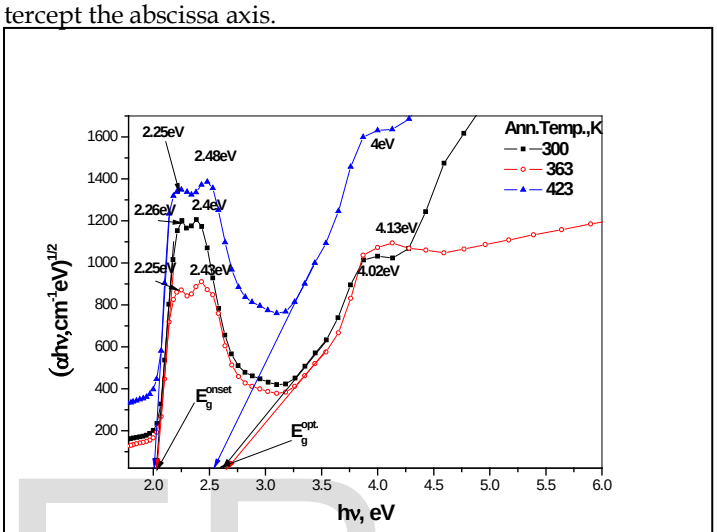

Fig. 8. The relation between $(ahv)^{1/2}$ and *hv* for RB thin films under different annealing temperatures.

The estimated values of the onset and the optical energy gap for pristine and annealed RB films are summarized in Table 2.

TABLE 2
DEPENDENCE OF THE ONSET AND THE OPTICAL ENERGY GAP FOR RB THIN FILMS ON THE ANNEALING TEMPERATURES.

Ann. temp. (K)	E_g^{onset} (eV)	$E_g^{opt.}$ (eV)
300	2.02	2.62
363	2.035	2.66
423	2.007	2.53

3.2.2 Dispersion, Dielectric and Optical Functions Characteristics of Annealed RB Films

Wemple and Di-Domenico [22] proposed the single oscillator model to explain the spectral dependence of refractive index in the transparent region of spectra; in this model the refractive index is related to the dispersion parameters by:

$$\frac{1}{n^2-1} = \frac{E_o}{E_d} - \frac{1}{E_o E_d}(h\upsilon)^2 \qquad (8)$$

where $h\upsilon$ is the photon energy, E_o is the oscillator energy that gives quantitative information on the overall band structure of the material and E_d is the dispersion energy which is a measure of the strength of inter-band optical transitions inside the material [23]. A plot of $(n^2\text{-}1)^{-1}$ versus $(h\upsilon)^2$ for RB films in the pristine and annealed conditions are illustrated in Fig. 9. The oscillator energy, E_o, and the dispersion energy, E_d, are directly determined from the slope $(E_o E_d)^{-1}$ of the linear portion of the curve and its intercept with ordinate axis (E_o / E_d).

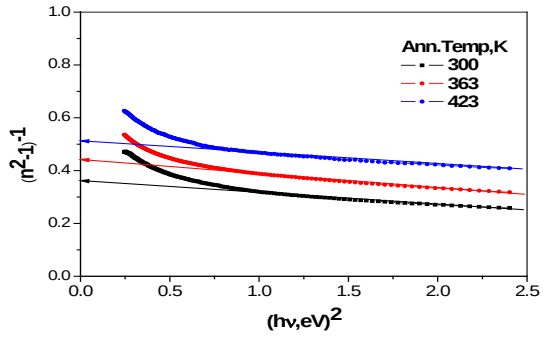

Fig. 9. The relation between $(n^2\text{-}1)^{-1}$ and $(h\upsilon)^2$ for annealed RB thin films.

The intercept of the linear portion of the curve with ordinate axis determines also the value of ε_∞ as well. The values of E_o, E_d and ε_∞ are summarized in Table 3.

TABLE 3
DISPERSION PARAMETERS OF PRISTINE AND ANNEALED RB THIN FILMS.

Ann.temp. (K)	ε_L	$_\infty\varepsilon$	$(N/m^*)\times10^{55}$ $(m^{-3}kg^{-1})$	E_0 (eV)	E_d (eV)
300	3.99	3.85	6.18	2.96	8.42
363	3.52	3.33	4.20	2.39	5.58
423	3.12	3.00	3.96	3.59	7.18

The real, ε_1, and imaginary, ε_2, components of the complex dielectric constant, ε^*, are given by [24]:

$$\varepsilon_1 = n^2 - k^2 = \varepsilon_L - \left(\frac{e^2}{4\pi^2 c^2 \varepsilon_o}\right)\left(\frac{N}{m^*}\right)\lambda^2, \qquad (9)$$

$$\varepsilon_2 = 2nk \qquad (10)$$

the parameter ε_L is the lattice dielectric constant, N/m^* is the ratio of the carrier concentration to the effective mass, e is the electron charge, c is the speed of light and ε_0 is the permittivity of free space. Since the extinction coefficient, k, is approaches zero in the transparent region of spectrum (Fig. 6), so a graphical representation of $n^2 \cong \varepsilon_1$ as a function of λ^2 for the pristine and annealed RB films is shown in Fig. 10. By extrapolating the linear part towards the shorter wavelength, the intercept with the ordinate axis (at $\lambda^2 = 0$) gives the value of ε_L and from the slopes of these lines the ratio N/m^* can be calculated. The calculated values of ε_L, ε_∞, N/m^* and the dispersion as well as the oscillator energies are given in Table 3.

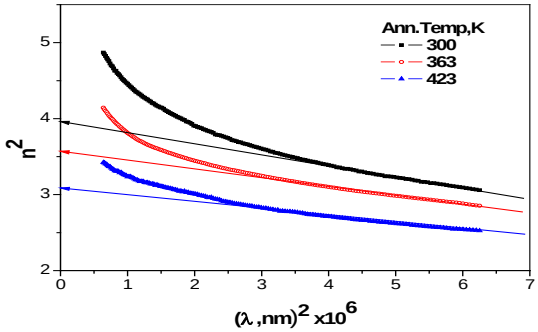

Fig. 10. The relation between n^2 versus λ^2 for annealed RB thin films.

The spectral distribution of ε_1 and ε_2 is represented in Figs. 11 and 12. It is clear that the values of ε1 are greater than the values of ε_2 at the same wavelength. The spectral distribution of ε_1 and ε_2, mainly can be divided into three regions depending on the energy of incident photons. Region I: is in the energy range < 2 eV at which a weak interaction occurs between the incident photons and electrons in RB films; and region II is in the energy range 2-2.6 eV and it represents the energy separation between the the onset and the optical energy gaps. In region II, ε1 decreases with increasing photon energy and ε_2 shows some bands representing the interactions of the incident photons with defects in the energy gap. Region III is in the energy range > 2.6 eV at which both of ε_1 and ε_2 increases with increasing photon energy. These results make us to believe that annealing temperatures influence the interactions of the incident photons with the electrons in RB films.

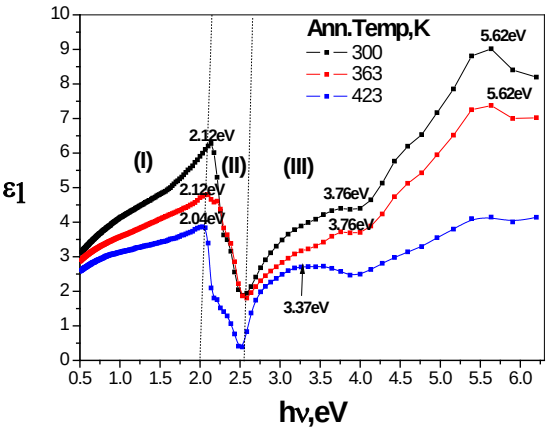

Fig. 11. The spectral distribution of ε_1 for annealed RB thin films.

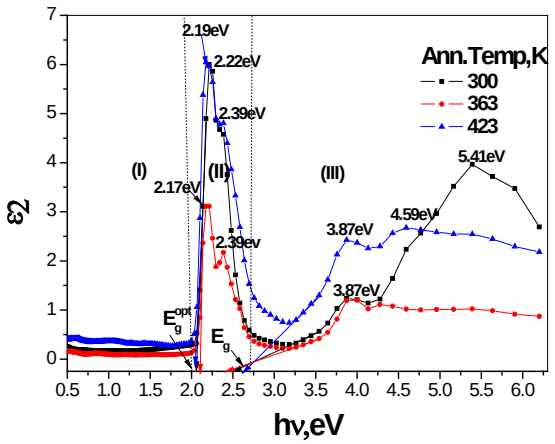

Fig. 12. The spectral distribution of ε_2 for annealed RB thin films.

The surface energy loss function, *SELF*, and the volume energy loss function, *VELF*, are related to the real and imaginary parts of the dielectric constant by the following relationships [25]:

$$SELF = \frac{\varepsilon_2}{(\varepsilon_1+1)^2+\varepsilon_2^2} \quad (11)$$

$$VELF = \frac{\varepsilon_2}{(\varepsilon_1^2+\varepsilon_2^2)} \quad (12)$$

Figs. 13 and 14 show the surface energy loss, SEL, and the volume energy loss, VEL, as a function of the incident photon energy. Both of these functions have the same behavior and the energy lost by photons traveling through the material is greater than the energy lost by those passing by its surface.

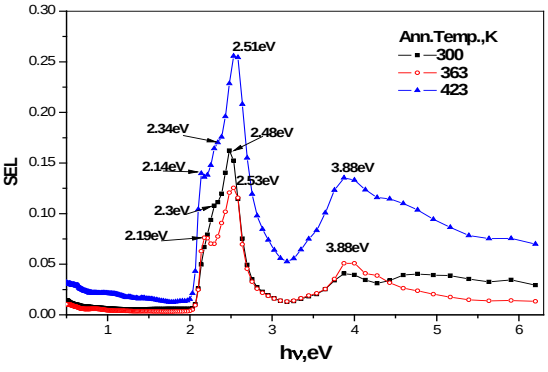

Fig. 13. The spectral distribution of surface energy loss for annealed RB thin films.

From Fig. 14, we can calculate the mobility, μ, of the charge carriers by applying the following relationship [26]:

$$\mu = \frac{e\tau}{m} \quad (13)$$

the parameter τ is the relaxation time which can be determined by using the relationship $(\omega_p \tau = 1)$ for the ω_p values obtained from the maximum peak values of Fig. 14. Table 4 summarize the values of μ, τ and ω_p for RB films in pristine and UV irradiated conditions.

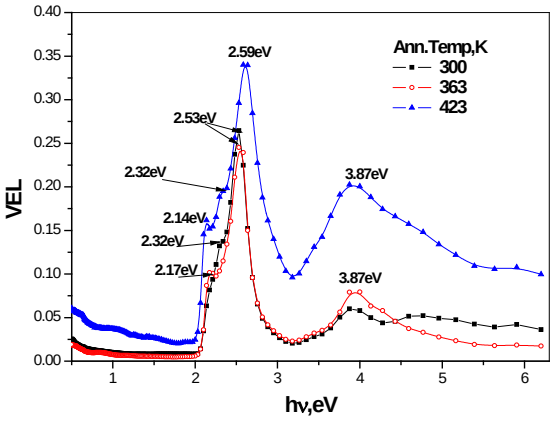

Fig. 14. The spectral distribution of volume energy loss for annealed RB thin films.

TABLE 4
EFFECT OF ANNEALING TEMPERATURES ON THE PLASMA FREQUENCY, ωP, RELAXATION TIME, T, AND MOBILITY M OF CHARGE CARRIERS OF RB THIN FILMS.

Ann. Temp. (K)	$\omega_p \times 10^{15}$ (Hz)	$\tau \times 10^{-15}$ (S)	$\mu \times 10^{-5}$ ($m^2V^{-1}S^{-1}$)
Pristine film	3.768	0.265	4.65
363	3.768	0.265	4.65
423	3.933	0.254	4.46

4 DISCUSSION

In this paper we report on the influence of annealing temperatures on the structure, optical and dielectrical properties of RB films. FTIR results shown in Table 1 illustrate that there are small shifts in the peak position of the absorption peaks. The data summarized in Table 1, indicates that there is no change in the chemical bonds of RB resulting either from spin coating or annealing process. The weak peak at 451-456 cm^{-1} is assigned to C-I and the vibration modes in the range 567-760 cm^{-1} are due to the multi C-Cl bonds. The absorption peak at 1613-1617 cm^{-1} is due to C=O stretching vibration. Results of Fig. 2 and Table 1, emphasis that the amorphous phase of RB film has the same chemical bonds as that of polycrystalline one. This indicates that RB film is chemically stable structure.

The endothermic peak observed in DSC curve of Fig. 3 at 357 K marks a transformation from amorphous solid phase to supercooled liquid state. The exothermic peak temperature T_p (598 K) is used to identify the melting temperature. The thermal analysis curves of Fig. 3 show that the RB films are thermally stable in the temperature range 300-590 K.

The diffraction peaks at 2θ angle of 29.9, 31.8 and 66° (Fig. 4d) indicate that the amorphous phase of powder, pristine and annealed (at 363 K) film of RB (Fig. 4a-c) becomes polycrystalline phase upon annealing at 463 K and this indicates that polymorphous crystallization occurred, where atoms in the disordered state jump to crystal front and those in clusters change their orientation to match the growing crystal and deposit onto the crystal front. The determined crystallite size of annealed RB film at 423 K is 230 nm. The transformation of amorphous structure of RB to polycrystalline structure (Fig. 4d) upon annealing at 423 K illustrates that a stable structure and a reduction of the structural disorder are attained.

The absence of any new peaks in the transmission and the reflection spectra in the absorption region as a result of the annealing process indicates that annealing temperatures have no effect on the transmittance and the reflectance properties of films. The transmission band, in the wavelength range 315-495 nm of Fig. 5, is strongly recommended RB films for application as an optical filter material.

The bands observed in anomalous dispersion region, Fig. 6, can be explained using multioscilattor model and they are attributed to electronic transition across π–π^* orbital [27]. The spectral behavior of n at normal dispersion region can be explained by adopting the single oscillator model, in this region, we can deduce the optical functions and the oscillator parameters at high frequencies. The decrease of refractive index, n, by annealing is a resulting of the decrease in the mass density [28]. The decrease in the density of RB films results from the release of moisture in temperature range 300-357 K as shown in Fig. 3. The doublet peak in the visible region of spectra of extinction coefficient k (Fig. 6) has been reported for RB by many authors [29-31]. According to multi oscillator model these peaks are attributed to the electronic transitions from bonding to anti-bonding molecular orbital [32, 33].

Pristine RB films have a remarkable high absorption coefficient (6×10^5 cm^{-1} at 2.24 eV) in the UV-vis. region of spectra. The absorption coefficient of the polycrystalline structure of the RB film is greater than its counterpart of the amorphous RB film, as shown in Fig. 7. Annealing temperatures have a different effect on the spectral distribution of α. Annealing RB films at 363 K decreases values of α all over the spectra, and this could be due to the fact that the annealing temperature of 363 K is near from the T_g where transformation from amorphous solid phase to supercooled liquid state occurs, i.e. rearrangement of atoms occurs and the matrix is still having amorphous structure. Annealing RB films at 423 K increases α all over the spectra and this is attributed to the formation of polycrystalline structure RB film. Hindeleh et al. [34] reported that the crystallite size influences the absorption of a material where small crystallites size has high absorption values.

The onset energy gap corresponds to the optical absorption, formation of vacancies, interstials, Frenkel pairs and dislocations in the films [35]. The optical energy gap is the energy gap between HOMO-LUMO bands [36]. The values of $E_g^{onset.}$ and $E_g^{opt.}$ for the pristine and annealed RB thin films are listed in Table 2. As can be observed from Table 2 and Fig. 9, the annealing at 423 K decreases $E_g^{onset.}$ and $E_g^{opt.}$. The decrease in onset and optical band gaps by annealing temperatures may be explained on the basis of the "density of state model" [37], in which, the width of the localized states near the mobility edges depends on the degree of disorder and defects present in the amorphous structure. In particular, it is known that unsaturated bonds together with some saturated bonds are produced as a result of an insufficient number of atoms deposited in the amorphous film [38]. The unsaturated bonds are responsible for the formation of some of the defects in the films, producing localized states in the amorphous solids. The presence of high concentration of localized states in the band structure is responsible for the decrease of optical band gap in the case of amorphous films. The decrease in the band gap may also be due to the shift in Fermi level, whose position is determined by the distribution of electrons over the localized states [39]. The decrease of the band gap with increasing annealing temperature is attributed to the reduction in disorder in the atomic bonding between neighbors resulting in a decrease of the density of tail states adjacent to the band edge and also attributed to the amorphous-polycrystalline transformations.

The oscillator energy E_o and the dispersion energy E_d have been reported to be related to the bond length L in the way. $E_o \propto L^{-s}$ [40] and E_d depends on L^s [41], with s varying in the range $2 < s > 3$ [40]. The variation of E_o and E_d with annealing temperatures may be interpreted on the basis that annealing temperatures induced partial transformation of the amorphous structure of RB into polycrystalline structure (Fig. 4d) and this requires displacing host atoms and rearranging of the bonds which results in influencing bond length with a degree depending on the annealing temperature.

Dielectric function relates the electron transitions between bands of a solid to its structure; therefore, we can obtain valuable information about the band structure of a solid from dielectric spectrum. The real dielectric constant shows different response to the increase of photon energy and annealing temperatures. Absorption peaks for ε1 are observed at 2.12, 3.76 and 5.62 eV for the as deposited and annealed (363 K) film, those films have an amorphous structure as shown in Fig. 4a-c, and at 2.04, 3.37 and 5.62 eV for the annealed RB films at 423 K; at which RB film shows a polycrystalline structure, Fig. 4d. The decrease of ε_1 with increasing annealing temperature is attributed to the decrease of the ratio of carrier concentration to its effective mass as shown in Table 3. The result of ε_2 shows different response to incident photon energy and annealing temperatures. Fig. 12 illustrates that the polycrystalline structure (annealing temperature 423 K) has greater value of ε_2 than those for amorphous structure of pristine and annealed (363 K) films. Therefore, we can gather conclude that the optical absorption edge depends on the annealing temperature of RB films. The onset and the optical energy gaps are determined from the intersection of the straight portions of bands with the abscissa axis as shown in Fig. 12. Their values correspond to those values listed in Table 2.

The electrical polarization takes place through four different mechanisms [42]. These mechanisms are: electronic, orientation, ionic and pace charge polarizations. The net polarization of the material is due to the contribution of all four-polarization mechanisms. The increase of ε_1 with photon energy can be attributed to the fact that at low frequencies (region I) ε_1 for polar materials is due to the contribution of multi com-

ponent of polarization, deformation polarization (electronic and ionic) and relaxation polarization (orientation and interfacial). When the frequency is increased, some of the dipoles can orient themselves sufficiently so that their oscillations reinforce those of the field. In region II, there are no charge carriers; therefore ε_1 decreases with increasing frequency. In region III, orientation and ionic polarizations take place and ε_1 increase with frequency.

Electron-energy-loss spectroscopy has been realized as important probes of the dielectric response of solids and the intrinsic statistical nature of the particle penetrating phenomena. The energy loss functions provide a complete description of the response of the material to ionizing particles or photons traveling either through its bulk or on its surface. It is clear from figs. 13 and 14 that both of *VELF* and *SELF* follow the spectral behavior of ε_2 and no effect of annealing temperatures on the spectral behavior of *VELF* and *SELF* functions. The change in their values upon annealing temperatures can be explained in terms of the structural changes occurred in RB films as shown in Fig. 3.

5 CONCLUSIONS

RB has an amorphous structure in the powder, pristine and annealed (363 K) film forms. The amorphous structure of RB films become polycrystalline structure upon annealing at 423 K. The data of T and R showed that the homogenous optical flat films are obtained by the spin coating technique and these films can be applied as an optical filter material. The type of electron transition in RB film is indirect allowed and the value of onset and optical energy gap is 2.02 and 2.59 eV, respectively. Annealing at 423 K decreases the onset and optical energy gap to 2.0 and 2.53 eV, respectively. The values of the lattice dielectric constant, the dielectric constant at infinite frequency, the ratio of carrier concentration to the effective mass and the dispersion energy are higher in amorphous structure film than those for polycrystalline structure one. The relaxation time, τ, and the mobility μ of the charge carriers of RB thin films decrease with increasing the annealing temperatures and the plasma frequency, ω_p, increases.

REFERENCES

[1] S. Sahu, D. Fujita, Y. Wakayama, Chem. Phys. 12 (2010) 2198.
[2] G.D. Sharma, P. Balraju, S. K. Sharma, M. S. Roy, J. Phys. Chem Solids 70 (2009) 1422.
[3] B. pradhan, S.-K. Batabyal, A.-J. Pal, Sol. Energy Mater Sol Cells 91 (2007) 769.
[4] M.S. Roy, P. Balraja, M. Kumar, G. D. Sharma. Sol. Energy Mater Sol. Cells 92 (2008) 909.
[5] K. M. Gangotri, M. K. Bhimwal, Sol. Energy 84 (2010) 1294.
[6] G. Zhao, H. Koyuka, T. Yoko, Sol. Energy Mater Sol. Cells 46 (1197) 219.
[7] M. Szaheloki, R. Luehowski, Z. Gryczynski, P. Kapusta, U. Ortmann, I. Grycnski, Chem. Phys. Letters 471 (2009) 153.
[8] A.K. Jana, J. Photochem. Photobiol. A Chem. 132 (2000) 1.
[9] L. Bahadur, L. Roy, J. Appl. Electro chem. 29 (1999) 109.
[10] Y.-S. Kim, V. Rubio, J. Qi, R. Xia, Z.-z. Shi, L. Peterson, C.-H. Tung, B. E. O'Neill, Journal of Controlled Release 156 (2011) 315.
[11] J.-H. Wang, B. Wang, Q. Liu, Q. Li, H. Huang, L. Song, T.-Y. Sun, H. Wang, X.- F. Yu, C. Li, P. K. Chu, Biomaterials 34 (2013) 4274.
[12] C.-C. Chang, Y.-T. Yang, J.-C Yang, H.-D. Wu, T. Tsai, Dyes Pigments 79 (2008) 170.
[13] A. A. Hamza, M. A. Mabrouk, W. A. Ramadan, A. M. Emara, Opt. Commu. 225 (2003) 341.
[14] L. A. Agiev, I. N. Shklyarevskii, J. Prekl. Spekt. 76 (1978) 380.
[15] H. M. Zeyada , M. M. EL-Nahass , I. S. Elashmawi , A. A. Habashi, J. Non-Cryst. Solids 358 (2012) 625.
[16] M. Fox "Optical Properties of Solids" Oxford University press, 2001.
[17] I. Konstantinov, T. Babeva, S. Ktova, Appl. Opt. 37 (1998) 4260.
[18] E. C. Raqueza, A. P. de Aguiar, M. R. M. P. de Aguiar, L. C. de Santa Maria, Thermochim. Acta 456 (2007) 128.
[19] T. J. Xue, M.A. Mckinneg, C.A. Wikie, Polym. Degrad. Stab. 58 (1997) 193.
[20] B.D. Cullity, "Elements of X-ray Diffraction", Addison-Wesley Publishing company, Inc., 1978.
[21] J. Tauc "Amorphous and liquid semiconductors" plenum press, London, 1974.
[22] S.H. Wemple, M. Di Domenico, Phys. Rev. B 3(4) (1971) 1338.
[23] I. Solomon, M. P. Schmidt, C. Sénémaud, M. D. Khodja, Phys. Rev. B 38 (1988) 1326.
[24] P.O. Edward, Hand Book of Optical Constants of Solids, Academic Press, New York, 1985.
[25] M. M. El- Nahass, Z. El-Gohary, H. S. Soliman, Opt. Laser Technol. 35 (2003) 523.
[26] H. M. Zeyada, N. A. El-Ghamaz, E.A. Gaml, Curr. Appl. Phys. 13 (2013) 1960.
[27] A. S. Davydov, "Theory of Molecular Excitons", Plenum press, New York, 1971.
[28] B. Andreas, I. Breunig, D. K. Buse, Chem. Phys. Chem. 6 (2005) 1.
[29] G. D. Sharma, P. Balraju, S. K. Sharma, M. S. Roy, J. Phys. Chem. Solids 70 (2009) 1422.
[30] M. S. Roy, P. Balraju, M. Kumar, G. D. Sharma, Sol. Energy Mater. & Sol. Cells 92 (2008) 909.
[31] B. Pradhan, A. J. Pal, Sol. Energy Mater. & Sol. Cells 81 (2004) 469.
[32] A. El-Korashy, H. El-Zahed, M. Radwan, Physica B 334 (2003) 75.
[33] H. M. El-Mallah, N. A. El-Ghamaz, M.A. Waly, J. Phys. D: Appl. Phys. 43 (2010) 455407.
[34] A. M. Hindeleh, M. A. Abdallah, N. S. Braik, J. Mater. Sci. 25 (1990) 1808.
[35] E. V. Tsiper, Z. G. Soos, W. Gao, A. Kahn, Chem. Phys. Lett. 360 (2002) 47.
[36] U. Zhokhavets, R. Goildhahn, G. Gobsch, W. Schliefke, Synth. Met. 138 (2003) 47.
[37] N. F. Mott, E. A. Davis." Electronic processes in non-crystalline Materials". Oxford: Clarendon, 1979, p. 428.
[38] Theye ML. Proc. Vth Int. Conf. Amorphous Liquid Semiconductors, 1973.
[39] T.T. Nang, M. Okuda, T. Matsushita, S. Yokota, A. Suzuki. Japanese J. Appl. Phys. 1976, 14: 849.
[40] H. Chen, W. Z. Shen, Eur. Phys. J. B 43 (2005) 503.
[41] J. M. Gonzalez-Leal, J. A. Angel, E. Marquez, R. Jimenez-Garay, J. Phys. Chem. Solids 68 (2007) 987.
[42] G. G. Raju, Dielectrics in Electric Field, Marcel Dekker, New York, 2003.